Compressive Failure as a Critical Transition: Experimental Evidence and Mapping onto the Universality Class of Depinning

Chi-Cong Vu, David Amitrano, Olivier Ple, Jérôme Weiss

Compressive Failure as a Critical Transition: Experimental Evidence and Mapping onto the Universality Class of Depinning

Chi-Cong Vu,[1] David Amitrano,[1] Olivier Plé,[2] and Jérôme Weiss[1,*]
[1]University of Grenoble Alpes, CNRS, ISTerre, 38000 Grenoble, France
[2]University of Savoie Mont-Blanc, CNRS, LOCIE, 73736 Le Bourget du Lac Cedex, France

(Received 17 July 2018; revised manuscript received 13 September 2018; published 10 January 2019)

Acoustic emission (AE) measurements performed during the compressive loading of concrete samples with three different microstructures (aggregate sizes and porosity) and four sample sizes revealed that failure is preceded by an acceleration of the rate of fracturing events, power law distributions of AE energies and durations near failure, and a divergence of the fracturing correlation length and time towards failure. This argues for an interpretation of compressive failure of disordered materials as a critical transition between an intact and a failed state. The associated critical exponents were found to be independent of sample size and microstructural disorder and close to mean-field depinning values. Although compressive failure differs from classical depinning in several respects, including the nature of the elastic redistribution kernel, an analogy between the two processes allows deriving (finite-) sizing effects on strength that match our extensive data set. This critical interpretation of failure may have also important consequences in terms of natural hazards forecasting, such as volcanic eruptions, landslides, or cliff collapses.

DOI: 10.1103/PhysRevLett.122.015502

Classical fracture and failure theoretical frameworks or criteria, such as Griffith theory or the Coulomb failure criterion, do not consider material disorder. Consequently, they predict an abrupt global failure, without any precursory phenomenon. In that sense, failure can be interpreted as a first-order transition from an intact to a failed state, as Griffith theory was inspired by the classical theory of nucleation [1,2]. Materials heterogeneity has been, however, considered for a long time, especially to account for failure strength variability and associated size effects [3]. Nevertheless, this weakest-link approach is based on strong assumptions, such as the absence of mechanical interactions between defects and between rupture events or a global failure dictated by the activation of the largest flaw (the weakest link). These assumptions might appear reasonable for weakly disordered materials under tension, especially in the case of a preexisting large crack or notch. However, in the case of a large enough disorder, the quasistatic propagation of such a crack can be interpreted as a dynamical critical transition [4,5]. The limitations of these classical frameworks appear even clearer for highly disordered systems without macroscale heterogeneities [6] and/or loading conditions stabilizing crack propagation, such as compression (through the presence of friction). In those cases, it has been known for a long time that failure is a *process*, involving the nucleation, interaction, propagation, and coalescence of many microcracks [7,8], hence characterized by precursory phenomena. The presence or absence of precursors to failure and faulting has obvious consequences in terms of natural hazards forecasting, for, e.g., earthquakes [9,10], cliff collapses [11], landslides [12], or volcanic eruptions [13,14].

The failure of heterogeneous media has been extensively studied over the last 30 years [1,15], essentially on the basis of theoretical and numerical models such as fiber-bundle (FBM) [16], random-fuse (RFM), random-spring (RSM) [17], or progressive damage (PDM) [2,18,19] models. However, the nature of the associated transition remains controversial. In the limit of infinite disorder, fracture can be mapped onto the percolation problem [20]. For bounded disorder, a FBM with equal-load sharing, corresponding to a mean-field approximation, exhibits a critical behavior with the rate of bundle breaking per increasing stress diverging at the critical point (the failure) [16]. A critical transition was also reported for a PDM of compressive faulting, with the average damage avalanche size, the correlation length of damage [19], or the largest damage cluster [2] all progressively increasing during the loading history and diverging at failure. This interpretation is also consistent with a mapping of the faulting problem onto the depinning transition [21]. On the other hand, for RFM and RSM with large (but finite) disorder, it has been claimed that there is no diverging correlation length at failure [17,22], consistent with a first-order transition interpretation of failure in those models [23]. Besides the nature of the transition, this raises the question of the role of the disorder strength on failure precursors.

This debate calls for experimental data, which are still sparse and disparate. Power law distributions of acoustic emission (AE) energies released by damage and

microcracking, $P(E) \sim E^{-\beta}$, have been frequently reported and presented as evidences of "criticality" in a broad sense. For highly porous [24,25] or cellular [26] materials under compression, the AE event rate dN/dt or the energy distribution do not exhibit significant trends as approaching failure, possibly as the result of a transient hardening mechanism [27], whereas the (stable) power law probability density function (PDF) of energies is accompanied by Omori-like aftershocks triggering. However, other authors reported an acceleration of the event rate (time-reversed Omori's scaling) towards failure for materials with a porosity larger than 30%, but an exponential growth (hardly compatible with the critical point hypothesis) for lower porosities [28,29]. In low-porosity rocks, a progressive localization of damage before faulting under compression has been revealed from either AE [7,30] or x-ray tomography [31,32]. In this last case, the damage rate, defined as the rate of increasing crack-induced porosity, as well as the size of the largest microcrack, were found to power law diverge as approaching global failure, arguing for an interpretation of compressive faulting as a critical transition [32]. Criticality was also argued for the flexural failure of composite materials from a divergence of the AE energy release [33].

Hence, despite these various hints, experimental evidence is still lacking to ascertain this critical interpretation of failure, determine the critical exponents, check their universal character, and precisely identify the role of internal disorder. To do so, we performed compression tests and AE measurements on an emblematic quasibrittle heterogeneous material, concrete. Cylindrical samples with a constant aspect ratio ($L/D = 2$) but four different sizes ($L = 80$, 140, 220, 320 mm) were prepared following French standards [34] and from three different concrete mixtures based on different aggregate sizes (fine F, i.e., only sand, medium M, and coarse C). Disorder consisted of aggregates, sand particles, and pores, with a larger porosity for F concrete ($\phi = 4.8\%$) than for M (1.6%) and C concrete (1.5%). The microstructures as well as the elastic properties were sample size independent, indicating that even the smallest samples were larger than the representative volume elements of the materials [35]. The preparation procedure and the microstructural characterization of our materials have been detailed elsewhere [35].

Uniaxial compression was applied on each sample at a constant stress rate of 0.5 MPa/s, corresponding to a strain rate between 2.4×10^{-5} and $3.2 \times 10^{-5}\ s^{-1}$. Loading was automatically stopped upon catastrophic failure, when the load dropped below 50% of peak load. Two (for $L =$ 80 mm samples) to four (for $L = 140$, 220, and 320 mm samples) piezoelectric AE sensors with a frequency bandwidth of 20–1200 kHz were coupled directly to the samples' sides using a silicon paste, and their signals were preamplified at 40 dB. A standard procedure was used to detect AE bursts over a 30 dB amplitude threshold, and their characteristics (maximum amplitude V_{max}, energy E, duration T) were saved. A scaling analysis between V_{max} and T (see Supplemental Material [36]) indicates that the recorded voltage $V(t)$ is a good proxy of the seismic moment release rate; i.e., T is a reasonable estimate of the duration of the fracturing event, for timescales larger than $\sim 100\ \mu s$. This allowed tracking the fracturing process up to macroscopic failure, materialized by the development of an inclined fault throughout the sample. For each material, four tests were performed for $L = 80$ mm samples and two tests for $L = 140$, 220, and 320 mm samples. The critical exponent values reported below result from an averaging over all these tests and all sensors.

We define the reduced control parameter as $\Delta = (\sigma_f - \sigma)/\sigma_f$, where σ_f is the peak (i.e. failure) stress, and conjecture that failure ($\Delta = 0$) is a critical point. Figure 1 shows the evolution of the intermittent AE activity during a typical test, where the event rate, total energy release, and maximum energy of events accelerate towards failure. Figure 2 shows the AE event rate diverging towards failure following $dN/d\Delta \sim \Delta^{-p}$ with a maximum likelihood estimate [14] of $p = 2/3 \pm 0.05$, independent of sample size [Fig. 2(a)] and material disorder [Fig. 2(b); see also Supplemental Material [36]]. Such time-reversed Omori's law [46] has been reported for the compressive failure of various porous materials ($14\% \leq \phi \leq 40\%$) [27–30,47], though with a varying p value, possibly depending on the strain rate [47]. In our low-porosity but disordered quasibrittle materials, under our stress-controlled protocol, p was found to be independent of both external and internal (disorder-related) scales.

This is accompanied by a progressive evolution of the distribution of AE energies as approaching failure

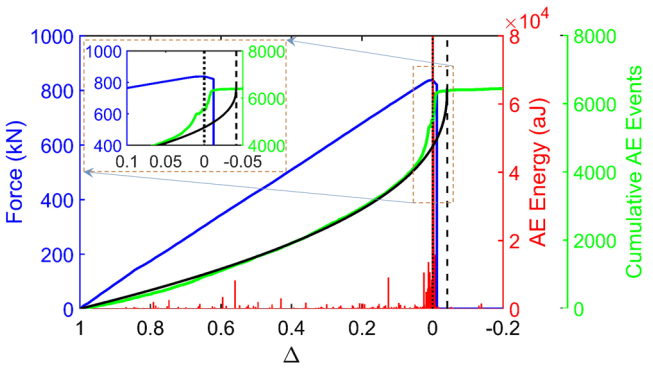

FIG. 1. Evolution of the AE activity during a stress-controlled compression test on a sample of length $L = 160$ mm of M concrete. (Blue curve) load; (green curve) cumulated number of AE events; (black curve) same as the green one for a theoretical time-reversed Omori's law with parameters estimated from a maximum likelihood method (see Supplemental Material [36]); (red) AE energy release rate, sampled at 100 Hz. The black dotted line represents the observed failure (maximum) stress, while the black dashed line represents the failure stress predicted from the theoretical time-reversed Omori's law.

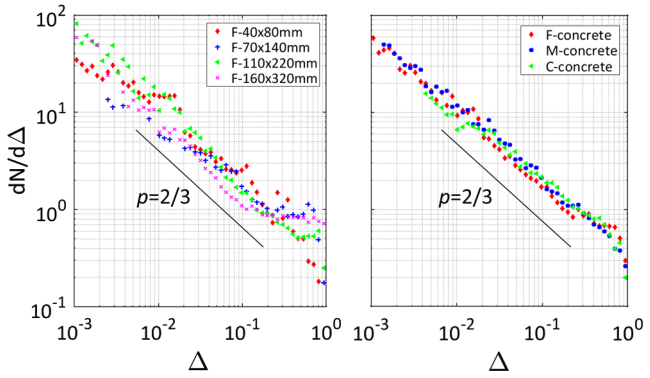

FIG. 2. AE event rate $dN/d\Delta$ (left) for different sample sizes of F concrete, and (right) for the three different materials. Curves on the left were averaged over all sensors and all samples of a given size and on the right on all sensors and samples (whatever the size) of a given material.

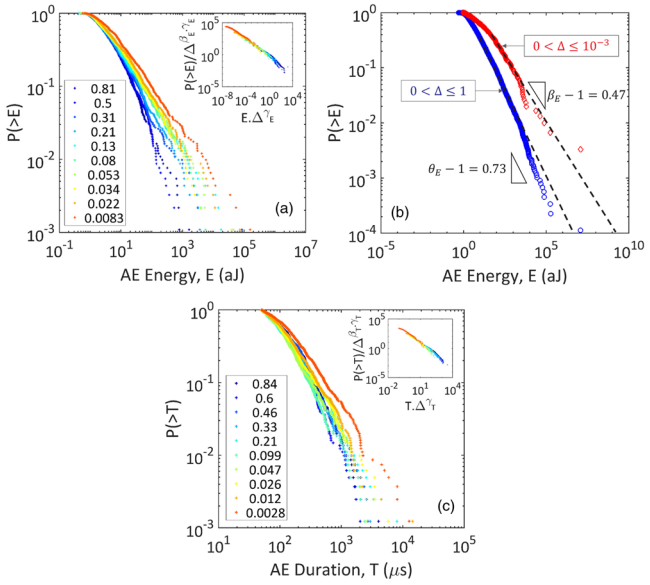

FIG. 3. Evolution of the distributions of AE energies and durations as approaching failure. (a) CDFs of AE energies at different distances to failure Δ, for a test on a 110 mm sample of M concrete. Each distribution is built from at least 300 events. (Inset) Data collapse of the same data in a rescaled plot. Other sample sizes and materials give similar results. (b) Near failure (red diamonds) and stress-integrated (blue circles) cumulative distribution of AE energies for a test on a 40 mm sample of F concrete. Other sample sizes and materials give similar results. (c) Same as (a) for the cumulative distributions of AE durations above 50 μs. At smaller timescales, the measured AE durations, influenced by wave scattering and seismic coda, are not a good proxy of avalanche durations (see Supplemental Material [36]).

[Fig. 3(a)]. In the early stages of loading, the energy cumulative distribution (CDF) $P(>E)$ is clearly truncated towards large energies, but the associated upper cutoff increases as fracturing goes on. Close to failure ($\Delta \to 0$), a power law CDF is recovered, $P(>E) \sim E^{-\beta+1}$, over ~5 orders of magnitude, without detectable upper cutoff [Fig. 3(a)]. We therefore conjecture an evolution of the PDF $P(E) \sim E^{-\beta_E} f(E/E^*)$, where $f(x)$ rapidly vanishes for $x > 1$ and a cutoff energy diverges at the critical point $E^* \sim \Delta^{-\gamma_E}$. From this, we recover a nontruncated power law distribution at failure $P(E) \sim E^{-\beta_E}$, while the sweeping of an instability [48] predicts another power law $P(E) \sim E^{-\theta_E}$ with $\theta_E = \beta_E + 1/\gamma_E$ for the stress-integrated PDF [Fig. 3(b)]. Our results support this conjecture with the exponents $\beta_E = 1.4 \pm 0.06$ and $\theta_E = 1.75 \pm 0.04$ not varying significantly with the sample size or the disorder. For each data set (one sensor on one sample), the exponents were determined from a maximum likelihood methodology [49]. This yields $\gamma_E = 1/(\theta_E - \beta_E) = 3.3 \pm 0.5$, a result that can be confirmed from a data collapse analysis [Fig. 3(a)]. Combined with inverse-Omori acceleration, this evolution of energy distributions, which itself means an increase of the average energy $\langle E \rangle$ towards failure, implies a divergence of the energy release rate $dE/d\Delta \sim \Delta^{-\alpha}$. We observed such evolution, independent of both sample size and disorder, however, with an exponent $a = 1.3 \pm 0.1$ smaller than expected from a simple analysis (see Supplemental Material [36]). Note that accelerations of the event rate and the energy release rate have been observed during the compressive failure of highly porous materials, although the energy distributions, and so $\langle E \rangle$, remained unchanged in this case. This indicates that these features are more generic than critical failure [27].

To translate this evolution of AE energies in terms of fracture size and correlation length, we consider an elastic crack model whose underlying hypotheses are (i) a compact (nonfractal) incremental crack or fault area A, (ii) an average slip or displacement proportional to the crack or fault "radius" $\langle u \rangle \sim r \sim A^{1/2}$, (iii) an r-independent stress drop, and (iv) a constant scaled energy, i.e., a radiated acoustic or seismic energy simply proportional to the potency $P_0 \sim \langle u \rangle A$ (or the seismic moment if multiplied by an elastic modulus). Such models are classical in AE analysis or seismology for both mode I cracks [50] or shear faults [51,52], well supported by available data [36], and lead to $E \sim r^3$ for the radiated acoustic energy. However, they differ from a depinning model of a planar fault [21,53] where the average slip $\langle u \rangle$ is independent of r, and ruptures can be fractal with $d_f \le 2$, hence $P_0 \sim r^{d_f}$. However, mean-field depinning also predicts a nonproportional scaling between the energy and the potency (or "size") of the avalanche $E \sim P_0^{3/2}$ [54,55]. Taking the limiting case $d_f \approx 2$, this gives $E \sim r^3$ as for elastic crack models, though from a subtly different framework. This scaling yields, for the cutoff incremental rupture radius, $r*^3 \sim E^* \sim \Delta^{-\gamma_E}$. Further identifying r^* with the correlation length ξ of the fracturing and faulting process, one gets a divergence $\xi \sim \Delta^{-\nu}$ with $\nu = \gamma_E/3 = 1.1 \pm 0.2$ for $\Delta \to 0$.

Similarly, an analysis of duration distributions during loading argues for a similar scaling $P(T) \sim T^{-\beta_T} g(T/T^*)$,

with a cutoff duration diverging at the critical point $T^* \sim \Delta^{-\gamma_T}$ and exponents $\beta_T = 2.0 \pm 0.15$, $\theta_T = 2.9 \pm 0.1$, and $\gamma_T = 1.1 \pm 0.3$ independent of disorder and sample size [Fig. 3(c)]. Although the uncertainty on these duration exponents is larger than for the energy distributions, this suggests $z = \gamma_T/\nu \approx 1$ for the dynamic exponent of the critical transition.

The power law distribution of microseismic energies and durations near failure, as well as the divergence of the rate of fracturing events, fracturing correlation length, and associated duration as approaching failure, are strong evidence for an interpretation of the compressive failure of low-porosity disordered materials as a critical transition, where the failure stress identifies as the critical point. This is further supported by the independence of the critical exponents relative to sample size and disorder. Theoretically, this critical interpretation could be checked from a finite-size scaling analysis of energy and duration PDFs obtained from samples of different sizes. We did not find, however, a fully convincing L dependence in our data, most likely because (i) the size range explored was limited ($L_{\max}/L_{\min} = 4$) and (ii) the necessarily limited experimental data statistics make the analysis of extremes difficult.

From these results, the nature of the critical transition and its possible affiliation to a particular universality class can be further discussed. A mapping of the problem of stick slip along an existing fault to the depinning of an elastic interface was proposed 20 years ago [21,53]. More recently, a similar analogy was proposed in case of compressive failure to account for statistical size effects on strength [56] (see below). Indeed, quasibrittle failure shares fundamental ingredients with the depinning transition, including a local threshold mechanism, disorder, and elastic interactions. Our results reveal a similar phenomenology of avalanches as approaching the critical point, with experimental exponents remarkably close to mean-field depinning ones [54,57,58] (see Supplemental Material [36]). On the other hand, several differences between the two problems can be stressed. First, the time-reversed Omori's scaling of the avalanche rate is not present in classical depinning, meaning that an additional exponent p is required to describe the failure transition. In addition, the nature of the elastic interaction kernel differs. Unlike for depinning, it is nonconvex in our case [56,59], allowing localization of damage along a fault, much like for the yielding transition in amorphous plasticity [60,61]. It is also non-negative, meaning that it has unstable modes, differing on this point from the yielding transition [59]. Although these differences preclude a direct affiliation of our problem onto the universality class of classical depinning, the scaling of the fracturing correlation length $\xi \sim \Delta^{-\nu}$, with an exponent very close to mean-field depinning ($\nu_{\mathrm{MF}} = 1$ [57]), suggests that some theoretical results could be tentatively transposed to our problem. In particular, we

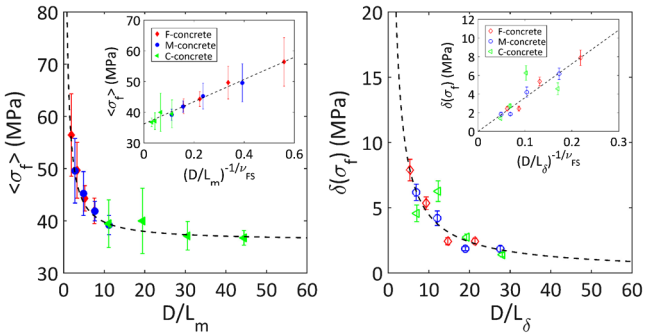

FIG. 4. Size effects on the average strength (left) and the associated standard deviation (right) of three types of concrete from a statistical data set of 527 compression tests. In these plots, the external sample diameter (D) is normalized by the internal (disorder-related) scales L_m (left) and L_δ (right), and the asymptotic material-independent strength is $\sigma_\infty = 36.2$ MPa. The dotted lines represent the finite-size scaling predictions with $\nu_{\mathrm{FS}} = 1.1$ (see text for details). (Insets) Same data in rescaled plots to show the asymptotic strength or the vanishing fluctuations towards the thermodynamic limit [$\lim_{L\to\infty}\delta(\sigma_f) = 0$].

can expect a finite-size effect on failure stress, yielding the following scaling laws for both the mean

$$\langle \sigma_f \rangle = \sigma_\infty (L/L_m)^{-1/\nu_{\mathrm{FS}}} + \sigma_\infty \tag{1}$$

and the standard deviation

$$\delta(\sigma_f) = \sigma_\infty (L/L_\delta)^{-1/\nu_{\mathrm{FS}}}, \tag{2}$$

where σ_∞ is the asymptotic strength of infinitely large systems, and L_m and L_δ are length scales related to the microstructural disorder characteristic length scale [56]. The classical assumption is $\nu_{\mathrm{FS}} = \nu$ [62], allowing one to relate the critical nature of the failure process to statistical size effects on strength. The above predictions were recently confirmed from an extensive series (527) of similar compression tests on the same materials and the same sample sizes (though without AE monitoring), using a mean-field depinning prediction for the exponent, $\nu_{\mathrm{FS}} = 1$ [35]. Here we reanalyzed these data using the AE-derived exponent $\nu_{\mathrm{FS}} = \nu = 1.1$. While the length scales L_m and L_δ (obtained from best fitting of the above equations with the data, taking $\nu_{\mathrm{FS}} = 1.1$) strongly depend on the material, and particularly its pore structure, the asymptotic strength σ_∞ was found to be essentially independent of the microstructural disorder. Consequently, the universal character of Eqs. (1) and (2) to account for experimental size effects on compressive strength of quasibrittle materials can be demonstrated on a rescaled plot (Fig. 4). Beyond an independent confirmation of the pertinence of the theoretical framework, these results strikingly illustrate the usefulness of statistical physics theoretical concepts accounting for the mechanical behavior of disordered

quasibrittle materials and, in the end, constrain engineering regulations [35].

The present work is also important in the context of a possible forecast of geophysical hazards. Time-reversed Omori's scaling has been proposed to forecast volcanic eruptions from seismic data [63], though with a large forecast uncertainty inherent in the form of this law (rate diverging towards the critical point) [14]. An evolution of the energy distribution of seismic signals, similar to that reported in Fig. 3(a), has been reported within 2 h before a chalk cliff collapse [11], but additional analysis would be needed to precisely check this analogy in terms of mechanisms and critical exponents. The possible prediction of large, devastating earthquakes is a long-standing, still unsolved problem. Many large earthquakes seem to be preceded by foreshocks, and a time-reversed Omori's law as well as a divergence of the seismic moment release rate have been sometimes reported [10]. However, these precursory phenomena are far from ubiquitous [9,64], and foreshocks could actually be just an expression of cascades of triggered seismicity implying that earthquakes are "predictable" to the same degree, whatever their size [65]. Hence, the use of these potential precursors as a forecasting tool remains elusive. This raises fundamental questions, such as the difference between the compressive failure of initially unfaulted rocks [31,32] and the earthquake nucleation along a preexisting crustal fault, and calls for further theoretical and experimental work as well as geophysical data analysis.

This work has been supported by the AGIR program (project SECRET) of Université Grenoble-Alpes. Anonymous referees are thanked for interesting comments and suggestions.

*jerome.weiss@univ-grenoble-alpes.fr

[1] M. J. Alava, P. K. V. V. Nukala, and S. Zapperi, Adv. Phys. **55**, 349 (2006).
[2] L. Girard, J. Weiss, and D. Amitrano, Phys. Rev. Lett. **108**, 225502 (2012).
[3] W. Weibull, Proc. R. Swed. Acad. Eng. Sci. **151**, 1 (1939).
[4] D. Bonamy, S. Santucci, and L. Ponson, Phys. Rev. Lett. **101**, 045501 (2008).
[5] J. Barés, L. Barbier, and D. Bonamy, Phys. Rev. Lett. **111**, 054301 (2013).
[6] J. Davidsen, G. Kwiatek, E.-M. Charalampidou, T. Goebel, S. Stanchits, M. Rück, and G. Dresen, Phys. Rev. Lett. **119**, 068501 (2017).
[7] D. A. Lockner, J. D. Byerlee, V. Kuksenko, A. Ponomarev, and A. Sidorin, Nature (London) **350**, 39 (1991).
[8] Z. e. Reches and D. A. Lockner, J. Geophys. Res. **99**, 18159 (1994).
[9] L. de Arcangelis, C. Godano, J. R. Grasso, and E. Lippiello, Phys. Rep. **628**, 1 (2016).
[10] S. C. Jaumé and L. R. Sykes, Pure Appl. Geophys. **155**, 279 (1999).
[11] D. Amitrano, J. R. Grasso, and G. Senfaute, Geophys. Res. Lett. **32**, GL08314 (2005).
[12] G. B. Crosta and F. Agliardi, Can. Geotech. J. **40**, 176 (2003).
[13] R. Sparks, Earth Planet. Sci. Lett. **210**, 1 (2003).
[14] A. F. Bell, M. Naylor, and I. G. Main, Geophys. J. Int. **194**, 1541 (2013).
[15] H. J. Herrmann and S. Roux, *Statistical Models for the Fracture of Disordered Media* (North-Holland, Amsterdam, 1990).
[16] S. Pradhan, A. Hansen, and B. K. Chakrabarti, Rev. Mod. Phys. **82**, 499 (2010).
[17] P. K. V. V. Nukala, S. Zapperi, and S. Simunovic, Phys. Rev. E **71**, 066106 (2005).
[18] D. Amitrano, J. R. Grasso, and D. Hantz, Geophys. Res. Lett. **26**, 2109 (1999).
[19] L. Girard, D. Amitrano, and J. Weiss, J. Stat. Mech. (2010) P01013.
[20] S. Roux, A. Hansen, H. Herrmann, and E. Guyon, J. Stat. Phys. **52**, 237 (1988).
[21] D. S. Fisher, K. Dahmen, S. Ramanathan, and Y. Ben-Zion, Phys. Rev. Lett. **78**, 4885 (1997).
[22] P. Nukala, S. Simunovic, and S. Zapperi, J. Stat. Mech. (2004) P08001.
[23] S. Zapperi, P. Ray, H. E. Stanley, and A. Vespignani, Phys. Rev. Lett. **78**, 1408 (1997).
[24] J. Baró, Á. Corral, X. Illa, A. Planes, E. K. H. Salje, W. Schranz, D. E. Soto-Parra, and E. Vives, Phys. Rev. Lett. **110**, 088702 (2013).
[25] G. F. Nataf, P. O. Castillo-Villa, P. Sellappan, W. M. Kriven, E. Vives, A. Planes, and E. K. H. Salje, J. Phys. Condens. Matter **26**, 275401 (2014).
[26] T. Mäkinen, A. Miksic, M. Ovaska, and M. J. Alava, Phys. Rev. Lett. **115**, 055501 (2015).
[27] J. Baró, K. A. Dahmen, J. Davidsen, A. Planes, P. O. Castillo, G. F. Nataf, E. K. H. Salje, and E. Vives, Phys. Rev. Lett. **120**, 245501 (2018).
[28] J. Vasseur, F. B. Wadsworth, Y. Lavallée, A. F. Bell, I. G. Main, and D. B. Dingwell, Sci. Rep. **5**, 13259 (2015).
[29] J. Vasseur, F. B. Wadsworth, M. J. Heap, I. G. Main, Y. Lavallée, and D. B. Dingwell, Earth Planet. Sci. Lett. **475**, 181 (2017).
[30] A. Schubnel, B. Thompson, J. Fortin, Y. Guéguen, and R. Young, Geophys. Res. Lett. **34**, L19307 (2007).
[31] F. Renard, B. Cordonnier, M. Kobchenko, N. Kandula, J. Weiss, and W. Zhu, Earth Planet. Sci. Lett. **476**, 69 (2017).
[32] F. Renard, J. Weiss, J. Mathiesen, Y. B. Zion, N. Kandula, and B. Cordonnier, J. Geophys. Res. **123**, 1969 (2018).
[33] A. Guarino, A. Garcimartin, and S. Ciliberto, Eur. Phys. J. B. **6**, 13 (1998).
[34] NF EN 206-1, 2004. Béton—Partie 1 : Spécification, Performances, Production et Conformité. Association Française de Normalisation (AFNOR).
[35] C. C. Vu, J. Weiss, O. Plé, D. Amitrano, and D. Vandembroucq, J. Mech. Phys. Solids **121**, 47 (2018).
[36] See Supplemental Material at http://link.aps.org/supplemental/10.1103/PhysRevLett.122.015502, which includes Refs. [37–45], for (i) a description of mechanical

tests and acoustic emission recording, (ii) an interpretation of AE durations, (iii) a table of critical exponents, (iv) details about the maximum likelihood estimation of the p value, (v) observational support for the crack or fault source model, (vi) details about AE energy release rate, and (vii) a brief discussion about the AE energy distributions.

[37] S. Deschanel, W. Ben Rhouma, and J. Weiss, Sci. Rep. **7**, 13680 (2017).
[38] C. H. Scholz and P. A. Cowie, Nature (London) **346**, 837 (1990).
[39] J. Walsh, J. Watterson, and G. Yielding, Nature (London) **351**, 391 (1991).
[40] S. Goodfellow and R. Young, Geophys. Res. Lett. **41**, 3422 (2014).
[41] E. J. Sellers, M. O. Kataka, and L. M. Linzer, J. Geophys. Res. **108**, 2418 (2003).
[42] H. Kanamori and E. E. Brodsky, Rep. Prog. Phys. **67**, 1429 (2004).
[43] I. G. Main, P. G. Meredith, and C. Jones, Geophys. J. Int. **96**, 131 (1989).
[44] X. Jiang, H. Liu, I. G. Main, and E. K. H. Salje, Phys. Rev. E **96**, 023004 (2017).
[45] D. Amitrano, Eur. Phys. J. Spec. Top. **205**, 199 (2012).
[46] T. Utsu, Y. Ogata, and R. Matsu'ura, J. Phys. Earth **43**, 1 (1995).
[47] I. O. Ojala, I. G. Main, and B. T. Ngwenya, Geophys. Res. Lett. **31**, L24617 (2004).
[48] D. Sornette, J. Phys. **4**, 209 (1994).
[49] A. Clauset, C. R. Shalizi, and M. E. J. Newman, SIAM Rev. **51**, 661 (2009).
[50] A. G. Evans, in *Fundamentals of Acoustic Emission*, edited by K. Ono (University of California, Los Angeles, 1979), p. 209.
[51] J. D. Eshelby, Proc. R. Soc. A **241**, 376 (1957).
[52] P. M. Shearer, *Introduction to Seismology* (Cambridge University Press, Cambridge, England, 2009).
[53] D. S. Fisher, Phys. Rep. **301**, 113 (1998).
[54] E. K. H. Salje and K. A. Dahmen, Annu. Rev. Condens. Matter Phys. **5**, 233 (2014).
[55] K. A. Dahmen, in *Avalanches in Functional Materials and Geophysics* (Springer, New York, 2017), p. 19.
[56] J. Weiss, L. Girard, F. Gimbert, D. Amitrano, and D. Vandembroucq, Proc. Natl. Acad. Sci. U.S.A. **111**, 6231 (2014).
[57] D. Ertas and M. Kardar, Phys. Rev. E **49**, R2532 (1994).
[58] M. LeBlanc, L. Angheluta, K. Dahmen, and N. Goldenfeld, Phys. Rev. E **87**, 022126 (2013).
[59] V. Démery, V. Dansereau, E. Berthier, L. Ponson, and J. Weiss, arXiv:1712.08537.
[60] J. Lin, E. Lerner, A. Rosso, and M. Wyart, Proc. Natl. Acad. Sci. U.S.A. **111**, 14382 (2014).
[61] B. Tyukodi, S. Patinet, S. Roux, and D. Vandembroucq, Phys. Rev. E **93**, 063005 (2016).
[62] O. Narayan and D. S. Fisher, Phys. Rev. B **48**, 7030 (1993).
[63] I. Main, Geophys. J. Int. **139**, F1 (1999).
[64] M. Bouchon, V. Durand, D. Marsan, H. Karabulut, and J. Schmittbuhl, Nat. Geosci. **6**, 299 (2013).
[65] A. Helmstetter and D. Sornette, J. Geophys. Res. **108**, 2483 (2003).